PHYSICAL REVIEW A **88**, 012702 (2013)

Feshbach projection approach to study plasma effects on doubly excited autoionizing states in helium

Andrés Felipe Ordóñez-Lasso,[1] Juan Carlos Cardona,[2] and José Luis Sanz-Vicario[1,*]

[1]*Grupo de Física Atómica y Molecular, Instituto de Física, Universidad de Antioquia UdeA, Calle 70 No. 52-21, Medellín, Colombia*

[2]*Grupo de Espectroscopía Óptica y Emisión Láser, Universidad del Atlántico, Barranquilla, Colombia*

(Received 28 May 2013; published 3 July 2013)

We have implemented a method based on the Feshbach formalism along with an explicitly correlated configuration interaction method to perform a systematic study on the behavior of resonance parameters (energies and lifetimes) of the autoionizing states of plasma-embedded He $^{1,3}S^e$, $^{1,3}P^o$, and $^{1,3}D^e$, as a function of the screening strength. In particular, we study the evolution of the lowest states in the series located below the $He^+(N=2)$ ionization threshold in the unscreened case. At variance with one-electron atoms (where shape resonance widths vary monotonically with the screening strength) the evolution of the Auger width with respect to screening is found to be different for each series represented by $(K,T)^A$ pseudoquantum numbers until resonances merge into the upper electronic continuum, when crossing the $He^+(2s)$ threshold. We conclude from our *ab initio* calculations that, although resonances pertaining to the same $(K,T)^A$ series share a similar tendency in their widths against the screening strength, general propensity rules for the robustness of lifetimes, based on the isomorphic series in the $(K,T)^A$ classification, cannot be established in plasma-embedded helium.

DOI: 10.1103/PhysRevA.88.012702 PACS number(s): 34.80.Dp, 32.80.Zb, 52.20.Fs

I. INTRODUCTION

The interest in the fundamental problem of atoms immersed in plasmas stems from its potential application in atomic, plasma, solid-state, and astrophysics. Formally, a plasma is characterized by a coupling constant γ, which refers to the ratio between the average Coulomb-interaction energy and the average kinetic energy [1]. The coupling constant for a plasma obeying the classical statistics at temperature T and atomic charge Z is $\gamma = (Ze)^2/k_BTa$, where $a = (4\pi n/3)^{-1/3}$ is the radius of a sphere with the characteristic volume $1/n$ (ion-sphere radius or Wigner-Seitz radius with the density n) and k_B is the Boltzmann constant. Most of the classical plasmas are weakly coupled plasmas with $\gamma \ll 1$ [1] (for instance, $n = 10^{11}$ cm^{-3} and $T = 10^4$ K for a gaseous-discharge plasma, $n = 10^{16}$ cm^{-3} and $T = 10^8$ K for a plasma in controlled thermonuclear fusion, or $n = 10^6$ cm^{-3} and $T = 10^6$ K for a plasma in the solar corona, for which $\gamma \sim 10^{-3}$, 10^{-5}, and 10^{-7} respectively).

Within the Debye-Hückel model [2] the plasma screening parameter λ corresponds to the inverse of the Debye characteristic length, $D = 1/\lambda = (k_BT/4\pi e^2 n)^{1/2}$, with the relevant parameters being the plasma temperature T and the plasma density n. The parameter D represents the free path length an electron is able to travel without being disturbed by plasma effects and it characterizes the strength of the coupling between the atomic species and the surrounding plasma. Since D is a function of T and n, a value for D corresponds to a wide range of plasma conditions. For $\gamma \geqslant 1$ the Debye-Hückel model may lose its validity and other models are more suitable (Debye-Laughton, ion-sphere, etc.). Atomic structure calculations using both the ion-sphere and the Debye-Hückel models can be found, for instance, in Ref. [3]. In this work, we restrict ourselves to the Debye-Hückel model, which is a good approximation to deal with static screening in weakly coupled plasmas near thermal equilibrium.

By using the Debye-Hückel model the effect of the plasma environment reduces to replace all the Coulomb two-particle interactions $\sim c/r_{ij}$ by an effective screened potential of the Yukawa type $\sim ce^{-\lambda r_{ij}}/r_{ij}$ (with screening parameter λ), whose effect is to shorten the range of the Coulomb potential. It is also worth noting that at variance with Coulomb potentials, in systems governed by Yukawa-like potentials the number of bound and resonant states is finite, thus without infinite Rydberg series. Atoms and molecules and their respective ions may show quite different energy spectra and properties while under the influence of an environment (caged atoms, plasma embedding, etc.). For instance, the ionization potential (IP) is strongly modified by the screening parameters, to the extreme in which the IP may become zero and the system cannot support bound states at all. At variance with isolated one-electron atoms, the problem of an electron subject to a Yukawa potential has no known analytical solution and its solution is limited to a variational quest. The effect of plasma screening on the ground state in helium was first approached by Rogers [4]. Lam and Varshi [5] also performed calculations for helium atom in a plasma, using a single-term explicitly correlated variational wave function and with angular momenta restricted to $(\ell_1,\ell_2,L) = (0,0,0)$, so that the two-electron shielded potential $e^{-\lambda r_{12}}/r_{12}$ was only expanded to lowest order $\ell = 0$. Nevertheless, they obtained a good estimation for the variation of the IP $= E[He^+(1s)] - E[He(1s^2)]$ with the screening parameter to find that for $\lambda \sim 1.74$ the IP becomes zero. This value was later corrected [6] to be slightly beyond $\lambda \sim 2.22$. In the present work we find this critical value for He close to $\lambda \sim 2.38$. Winkler [7] also calculated the detachment energies (IP) for the negative hydrogen ion in a Debye plasma, to state that for the screening parameter $\lambda \geqslant 1.14$ both H^- and H species simultaneously reach a vanishing IP and they do not support bound states anymore. In fact, the critical λ values for H^- and H are very close but they are not exactly equal. For

*Corresponding author: sanjose@fisica.udea.edu.co

instance, in the He and He^+ pair, at $\lambda > 2.38$ the He^+ ion may still have a binding potential up to the upper limit established by Brau and Calogero [8]. In general, the distance between critical values corresponding to the atom (or ion) $A^{(Z-2)+}$ and to the parent ion (or atom) $A^{(Z-1)+}$ along the Z-isoelectronic series depends upon the relation λ/Z.

Surprisingly, one-particle shape resonant states in the spherically symmetric Yukawa potential have not been studied until recently [9]. In this one-electron atom context, when λ increases a discrete bound state eventually reaches the ionization threshold and then changes its nature to be a resonance immersed in the electronic continuum; the presence of these kinds of resonances may notably change the photoabsorption cross sections near the resonant region. Bylicki *et al.* [9] found that the presence of bound states and resonances in one-electron atoms with nuclear charge Z depends upon only one parameter $p = \ell(\ell+1)\lambda/2Z$. If $p < 1/e$ the Yukawa potential may support both bound and resonant states. For $1/e \leqslant p \leqslant \frac{1}{2}(\rho_0^2+\rho_0)e^{-\rho_0}$, where $\rho_0 = \frac{1+\sqrt{5}}{2}$, only resonances exist and for $p > \frac{1}{2}(\rho_0^2+\rho_0)e^{-\rho_0}$ neither bound nor resonances are present in the energy spectrum. Such a clear distinction in terms of only one parameter p, the latter a function of the three parameters $\{\ell,\lambda,Z\}$, is no longer possible in many-electron atoms and the analysis requires explicit computations. In one-electron atoms the widths of the shape resonances always increase dramatically when the screening parameter λ increases [9].

In two-electron atomic systems, resonant states are usually classified into shape and Feshbach-Fano resonances, according to their location above or below a given ionization threshold, respectively. Below the threshold the autoionization process of a Feshbach resonance is entirely due to the correlation between the electrons. Above the threshold, the resonance phenomena are due to the temporal trapping of one electron when scattered from the effective potential of the target parent ion, whose energy corresponds to the given ionization threshold. Incidentally, increasing the Yukawa screening parameter in many-electron atoms represents an ideal situation in which one may expect to find threshold crossovers of bound and Feshbach resonant states transforming into shape resonances. Focusing on Feshbach resonances in plasma-embedded He, we show in this work that their widths notably modify as a function of the λ parameter, but they do not increase monotonically as a general rule. Instead, their variation depends on the type of resonance series corresponding to the labels $(K,T)^A$, according to the classification proposed by Lin [10], after the pioneering work of Herrick and Sinanoğlu [11]. Following the latter works, it is understood that whereas configurational states using single-electron quantum numbers, i.e., $|(n_1\ell_1,n_2\ell_2);^{2S+1}L^\pi\rangle$, are widely employed to label ground and singly excited states, a general classification of doubly excited states in terms of them mostly fails. At variance, a description in terms of two approximated angular quantum numbers (K,T) that replace the pair (ℓ_1,ℓ_2) notably improves the interpretation of the atomic resonant spectra since resonant properties are better classified and understood within (K,T) series. Of course, the transformation to the new dipolar basis set $|_{n_1}(K,T)_{n_2};^{2S+1}L^\pi\rangle$ leaves the total quantum numbers of the atomic state (L, S, and parity π) invariant. Lin [10] added the approximate radial quantum number A to distinguish different radial correlations in the wave functions; those wave functions with antinodal structure at $r_1 = r_2$ are assigned to $A = +1$, those with nodal structure at $r_1 = r_2$ have $A = -1$, and those with no definite parity at $r_1 = r_2$ have $A = 0$. Accordingly, we better adopt this *complete classification scheme* to label resonances within a given spectroscopical symmetry $^{2S+1}L^\pi$.

Recently, a plethora of papers released by the Y. K. Ho group have been dedicated to the study of bound and doubly excited states in two-electron atomic systems immersed in plasma environments (see [6,12–23] and references therein). In particular, Kar and Ho first dealt with the $2s^2\ ^1S^e$ resonance state without considering the screening between electrons in H^- [12], then including it for the lowest $^1S^e$ resonance in H^- [13], in He [14], and Ps^- [15]; they also studied the screening effect on $^{1,3}P^o$ [16,17] and $^{1,3}D^e$ resonances [23]. In these series of papers, the stabilization procedure [24] is widely used along with a configuration interaction (CI) method with explicitly correlated coordinates to uncover the resonances and to characterize their parameters by fitting the density of resonance states to a Lorentzian form. Usually, in the works by Ho *et al.* a ∼500- to 700-term explicitly correlated CI wave function is employed, with a scaling parameter ω that makes it possible to vary the basis in order to obtain the energy stabilization graphs. The stabilization method is a many-diagonalization procedure which requires fine-grained grids in the ω value (for instance, $\Delta\omega = 0.001$ from $\omega = 0.3$ to 1.0); i.e., it amounts to hundreds of diagonalizations for each value of the screening parameter λ, which reduces the computational effectiveness of the stabilization method in these kinds of systematic studies for an assortment of λ values. In this work, we propose the Feshbach partitioning projection method, which in practice requires only two diagonalizations per λ value, one for the resonant $\mathcal{Q}$ space and another for the nonresonant $\mathcal{P}$ space, also making use of explicitly correlated coordinates within a CI method. As a case study for the methodology, our aim is to analyze the behavior of energies and autoionizing widths of He $^{1,3}S^e$, $^{1,3}P^o$, and $^{1,3}D^e$ resonant states located below the second ionization threshold He^+ ($N = 2$) for $\lambda = 0$, when the screening strength λ is modified. It has been shown for $\lambda = 0$, using hyperspherical coordinates, that states with different angular momentum L, spin S, and parity π but identical $(K,T)^A$ labels have isomorphic correlation patterns [10]. One may wonder whether such isomorphic correlations partially survive for $\lambda \neq 0$ and induce a similar behavior for the lifetimes of resonances with the same $(K,T)^A$ labels against the variation of the screening strength.

The paper is organized as follows. In Sec. II we describe the theoretical approach, including a short description of the implementation of the Feshbach approach and the computational details. In Sec. III we present our results for the energies, widths, and the interelectronic angle as a function of the screening parameter. We end up with some conclusions and perspectives in Sec. IV. Atomic units (a.u.) are used unless otherwise stated.

II. THEORY

The Hamiltonian for a nonrelativistic two-electron system embedded in a weakly coupled plasma characterized by the screening parameter λ and when using trial wave functions that

depend on coordinates $\{r_1,r_2,r_{12},\Omega_1,\Omega_2\}$, with $\Omega_i = (\theta_i,\phi_i)$, reads

$$\begin{aligned}\hat{H} = &-\frac{1}{2}\sum_{i=1}^{2}\left[\frac{\partial^2}{\partial r_i^2}+\frac{2}{r_i}\frac{\partial}{\partial r_i}-\frac{\ell_i(\ell_i+1)}{r_i^2}\right]\\ &-\left[\frac{\partial^2}{\partial r_{12}^2}+\frac{2}{r_{12}}\frac{\partial}{\partial r_{12}}\right]\\ &-\frac{1}{2}\left[\frac{r_1^2-r_2^2+r_{12}^2}{r_1 r_{12}}\frac{\partial^2}{\partial r_1\partial r_{12}}+\frac{r_2^2-r_1^2+r_{12}^2}{r_2 r_{12}}\frac{\partial^2}{\partial r_2\partial r_{12}}\right]\\ &+\left[\frac{r_2}{r_1 r_{12}}\left(\hat{\mathbf{r}}_2\cdot\hat{\nabla}_1^Y\right)\frac{\partial}{\partial r_{12}}+\frac{r_1}{r_2 r_{12}}\left(\hat{\mathbf{r}}_1\cdot\hat{\nabla}_2^Y\right)\frac{\partial}{\partial r_{12}}\right]\\ &-\frac{Z\exp(-\lambda r_1)}{r_1}-\frac{Z\exp(-\lambda r_2)}{r_2}+\frac{\exp(-\lambda r_{12})}{r_{12}},\end{aligned}\tag{1}$$

an expression in which $\hat{\mathbf{r}}_i = \mathbf{r}_i/r_i$ is a unit vector and $\hat{\nabla}_i^Y = r_i\nabla_i^Y$, where ∇_i^Y corresponds to the angular part of the gradient operator. We have previously used a similar Hamiltonian in our Hylleraas configuration interaction (HyCI) approach to compute resonances in berylliumlike atoms [25], but where Coulomb interactions are now replaced with screened Yukawa-like interactions. In that previous work [25] we built all ingredients necessary to uncover resonant states in isolated Be-like atoms by implementing the stabilization procedure. For the reasons stated in the Introduction we now choose instead the Feshbach approach.

A. Feshbach projection formalism

The Feshbach projection method [26,27] provides a powerful method to deal with resonance phenomena in scattering processes. Most of the known applications in atomic and molecular physics are reduced to two-electron (see, for instance, [27] and references therein) and three-electron systems [28,29]. Additionally, it has shown to be a remarkable method not only as a time-independent approach but also in the time domain [30,31]. For the sake of completeness, we give here a brief review of the Feshbach method as applied to two-electron atoms. The Feshbach projection operator formalism introduces two projection operators, $\mathcal{P}$ and $\mathcal{Q}$, which satisfy completeness ($\mathcal{P}+\mathcal{Q}=1$), idempotency ($\mathcal{P}^2=\mathcal{P}$, $\mathcal{Q}^2=\mathcal{Q}$), and orthogonality ($\mathcal{P}\mathcal{Q}=\mathcal{Q}\mathcal{P}=0$) and project the total wave function onto nonresonant scatteringlike $\mathcal{P}$ and boundlike $\mathcal{Q}$ half spaces, respectively. Accordingly, the splitting of the total continuum wave function reads $\Psi = \mathcal{P}\Psi + \mathcal{Q}\Psi$ and it can be substituted in the Schrödinger equation $H\Psi = E\Psi$ to obtain a system of coupled equations,

$$(E-\mathcal{Q}H\mathcal{Q})\mathcal{Q}\Psi = \mathcal{Q}H\mathcal{P}\Psi,\tag{2a}$$

$$(E-\mathcal{P}H\mathcal{P})\mathcal{P}\Psi = \mathcal{P}H\mathcal{Q}\Psi.\tag{2b}$$

$\mathcal{Q}\Psi$ can be extracted formally from Eq. (2a) as $\mathcal{Q}\Psi = \mathcal{Q}H\mathcal{P}\Psi/\mathcal{Q}(E-H)\mathcal{Q}$ and then substituted in Eq. (2b) to obtain the following optical potential Schrödinger equation for $\mathcal{P}\Psi$:

$$\mathcal{P}\left[H+H\mathcal{Q}\frac{1}{\mathcal{Q}(E-H)\mathcal{Q}}\mathcal{Q}H-E\right]\mathcal{P}\Psi = 0.\tag{3}$$

Now the Green's function for $\mathcal{Q}$ space can be expanded in terms of the $\mathcal{Q}H\mathcal{Q}$ eigenvalues $\mathcal{E}_n$ and its eigenfunctions $\Phi_n \equiv \mathcal{Q}\Phi_n$, i.e., $(\mathcal{Q}H\mathcal{Q}-\mathcal{E}_n)\Phi_n = 0$, to yield

$$G_{\mathcal{Q}}(E) = \frac{1}{\mathcal{Q}(E-H)\mathcal{Q}} = \sum\!\!\!\!\!\!\int_n \frac{|\Phi_n\rangle\langle\Phi_n|}{E-\mathcal{E}_n}.\tag{4}$$

The *nonresonant* component of the continuum wave function, named $\mathcal{P}\Psi^0$, for an energy E close to the resonance state with energy $\mathcal{E}_s$ is obtained by removing the resonant component $n=s$ from Eq. (4) when substituted in Eq. (3). Then the Feshbach *static* working equations for the boundlike and the *nonresonant* scatteringlike parts are

$$(\mathcal{Q}H\mathcal{Q}-\mathcal{E}_n)\Phi_n = 0,\tag{5a}$$

$$(\mathcal{P}H'\mathcal{P}-E)\mathcal{P}\Psi^0 = 0,\tag{5b}$$

where H' is the operator containing the atomic Hamiltonian plus an optical potential devoid of any resonant contribution from the state Φ_s with energy $\mathcal{E}_s$, i.e., $H' = H + V_{\rm opt}^{n\neq s}$, where

$$V_{\rm opt}^{n\neq s} = \sum\!\!\!\!\!\!\int_{n\neq s} \mathcal{P}H\mathcal{Q}\frac{|\Phi_n\rangle\langle\Phi_n|}{E-\mathcal{E}_n}\mathcal{Q}H\mathcal{P}.\tag{6}$$

Within the Feshbach formalism the $\mathcal{Q}H\mathcal{Q}$ eigenvalues $\mathcal{E}_s$ must be corrected with an energy shift Δ_s (due to the surrounding continuum states), readily calculated with a second-order perturbation formula,

$$\Delta_s = \sum\!\!\!\!\!\!\int_{E'\neq\mathcal{E}_s} dE'\frac{|\langle\Phi_s|\mathcal{Q}H\mathcal{P}|\mathcal{P}\Psi^0(E')\rangle|^2}{\mathcal{E}_s-E'},\tag{7}$$

so that the resonance energy is actually corrected to be $E_s = \mathcal{E}_s+\Delta_s$. Also, the Auger width of a resonance with energy E_s is computed by using Fermi's golden rule,

$$\Gamma_s = 2\pi\rho(E=E_s)|\langle\Phi_s|\mathcal{Q}H\mathcal{P}|\mathcal{P}\Psi^0(E=E_s)\rangle|^2,\tag{8}$$

where $\rho(E)$ is the density of continuum states at the resonance energy. The application of Eq. (8) requires the evaluation of $\mathcal{Q}H\mathcal{P}$ matrix elements between $\mathcal{Q}$ and $\mathcal{P}$ wave functions having the same continuum energy. However, the computational solution of the $\mathcal{P}H\mathcal{P}$ problem with a finite basis set results in a discretized continuum. In general, none of the discretized continuum energies $\{E_i\}$ matches any resonance energy E_s. In order to get the energy matching, we use an inverse interpolation method [29,32].

In practice, one starts by first solving the $\mathcal{Q}H\mathcal{Q}$ problem (5a), which implies to use the two-electron projector $\mathcal{Q} = 1-\mathcal{P}$, where $\mathcal{P} = \mathcal{P}_1+\mathcal{P}_2-\mathcal{P}_1\mathcal{P}_2$, with $\mathcal{P}_i = |\phi_{1s}(i)\rangle\langle\phi_{1s}(i)|$ as the projector for electron i in the $1s$ orbital. The direct application of the projector $\mathcal{Q}$ is rather cumbersome and, instead, one may solve the easier but equivalent eigenvalue problem associated with the effective Hamiltonian $H_{\rm eff} = H+M\mathcal{P}$, where $M\mathcal{P}$ represents a Phillips-Kleinman pseudopotential [33], with $M\to\infty$ (in practice, M is a large positive real number). The operator $M\mathcal{P}$ projects upward in energy all eigenstates corresponding to the bound plus scatteringlike P half space, in such a way that the lowest eigenstates of $H_{\rm eff}$ now correspond to the Rydberg discrete series of resonant states below the second ionization threshold, if the explicit $\mathcal{P}_i$ expressed above is used. The $\mathcal{P}H'\mathcal{P}$ eigenproblem (5b) is solved by diagonalizing the full Hamiltonian H' in a $\mathcal{P}$-projected basis set of configurations, using the *static-exchange* approximation (in which the target He^+ is not excited), which

guarantees the orthogonality with the $\mathcal{Q}$-space wave functions (see, for instance, [29]).

B. Computational details

We use a HyCI method, where the total wave function is built up as a linear combination of antisymmetrized correlated configurations of the form $\psi_i(\mathbf{x}_1,\mathbf{x}_2) = \mathcal{A}\{\phi_i(\mathbf{r}_1,\mathbf{r}_2)\chi(s_1,s_2)\}$, with $\mathbf{x}_i \equiv (\mathbf{r}_i,s_i)$ for the spatial and spin electron coordinates. The spatial part of the wave function is built up in terms of correlated Slater-type orbitals,

$$\phi_i(\mathbf{r}_1,\mathbf{r}_2) = r_1^{n_1} r_2^{n_2} r_{12}^{n_{12}} \mathrm{e}^{-\alpha r_1-\beta r_2} \mathcal{Y}_{(\ell_1,\ell_2),L,M}(\Omega_1,\Omega_2), \quad (9)$$

where $\mathcal{Y}_{(\ell_1,\ell_2),L,M}(\Omega_1,\Omega_2)$ is a coupled product of spherical harmonics,

$$\mathcal{Y}_{(\ell_1,\ell_2),L,M}(\Omega_1,\Omega_2) = (-1)^{\ell_1-\ell_2+M}[L]^{1/2} \times \sum_{m_1,m_2} \begin{pmatrix} \ell_1 & \ell_2 & L \\ m_1 & m_2 & -M \end{pmatrix} Y_{\ell_1,m_1}(\Omega_1) Y_{\ell_2,m_2}(\Omega_2) \quad (10)$$

and $[L] \equiv (2L+1)$. In Eq. (9) the index i corresponds to the full set $[(n_1,n_2,n_{12},\alpha,\beta);(\ell_1,\ell_2)]$ that labels each correlated configuration entering the CI wave function. A detailed description to proceed with the (radial and angular) integrals involved in the general method as well as with the Feshbach projection may be found in Refs. [25,34], in which integrals involving screened Coulomb potentials were not considered. Nevertheless, the only new integral that involves the screened two-electron interaction term $e^{-\lambda r_{12}}/r_{12}$ can also be computed in closed analytical form following the ideas of the seminal paper by Calais and Löwdin [35] (see also [36,37]). Indeed, all these integrals can be written in terms of the array $[klm]$ of Eq. (28) in Ref. [35], which in our implementation are precomputed and kept in dynamical memory storage, once the full set of n_1, n_2, n_{12}, α,β, and λ values are selected for the basis set.

To construct the basis set we vary the set of powers n_1, n_2, n_{12} as follows: $n_i = \ell_i + j$, with $0 \leqslant \ell_i \leqslant 3$ (s,p,d,f); $0 \leqslant j \leqslant 3$; and $n_{12} \leqslant 2$. The nonlinear parameters α and β are varied following an even-tempered sequence of the form $\alpha^{(k,\ell)} = Z/\gamma^k(\ell+1)$, with $\gamma \in [2.0,3.2]$ to avoid linear dependencies. Accordingly, the $\mathcal{Q}H\mathcal{Q}$ eigenvalue problem is solved as follows (for instance, in the case of singlets): $^1S^e$ symmetry is computed with 420 ss, 210 pp, and 83 dd configurations (from which 210 ss, 84 pp, and 21 dd are explicitly correlated); the $^1D^e$ manifold of states is computed with 390 sd, 255 pp, and 225 pf configurations (180 sd, 120 pp, and 90 pf are explicitly correlated). Computations in terms of uncorrelated Slater-type orbitals may require many more configurations and a larger set of coupled angular configurations (ℓ_1,ℓ_2). In fact, the expansion of $r_{12}^{n_{12}}$ introduces additional angular correlation in the configurational basis. Incidentally, we find that explicitly correlated calculations for symmetry $^{1,3}P^o$ are much harder to perform due to difficulties associated to linear dependencies that prevent us from a rapid saturation of the basis. Then we have chosen instead uncorrelated configurations for $L = 1$. For instance, for the $^1P^o\mathcal{Q}H\mathcal{Q}$ eigenvalue problem we employed 273 sp, 210 pd, 126 df, and 126 fg uncorrelated configurations.

To build up the $\mathcal{P}$-projected basis we use the *static-exchange* approximation, in which one of the electrons is fixed to the core $He^+(1s)$. In practice, we use the same CI code but avoid correlated configurations (much less important for the continuum states) by building antisymmetrized configurations in the form $\mathcal{A}\{\varphi_{1s}^{\lambda}(r_1) f_i(r_2) \mathcal{Y}_{(\ell_1,\ell_2),L,M}(\Omega_1,\Omega_2)\chi(s_1,s_2)\}$, where φ_{1s}^{λ} corresponds to the radial function of the He^+ $(1s)$ state immersed in a plasma with screening parameter λ and $\{f_i\} = r^{L+n_i} e^{-\alpha_i r}$ is a Slater-type basis set that represents the scattered electron. At variance with He isolated atoms, in which the projector $\mathcal{P}$ is constructed exactly, in the plasma immersed He the projector is not exact but the orbital φ_{1s}^{λ} can be obtained accurately from variational calculations for each value of the screening parameter λ in terms of a Slater-type basis set; i.e., our one-particle projector is now $\mathcal{P}_i = |\varphi_{1s}^{\lambda}(i)\rangle\langle\varphi_{1s}^{\lambda}(i)|$. To simplify the Feshbach $\mathcal{P}$ projection procedure, we have used a hydrogenlike orbital with a single nonlinear parameter to model the $1s$ orbital, $\varphi_{1s}^{\lambda} = Ne^{-\alpha_\lambda r}$, where α_λ is optimized variationally and N is the normalization factor. For the range of screening parameters included in this work ($\lambda \in [0,0.5]$) there is an excellent match between this one-parameter wave function and the one obtained with a converged variational calculation using a large set of Slater-type orbitals (STOs). For instance, an uncorrelated calculation in $\mathcal{P}$-space for the nonresonant continuum in the $^1S^e$ symmetry makes use of 220 ss configurations, which means that a set of 220 STOs with $\ell = 0$ is employed to represent the scattered electron, whereas the target electron remains in the *screened* $1s$ orbital.

The implementation of our Feshbach method along with Hylleraas type coordinates is very efficient computationally. For instance, a complete computation for any of the $^{2S+1}L^{\pi}$ symmetries and for a set of 50 parameters $\lambda \in [0,0.5]$ takes less than 6 h in a desktop computer with a sequential 3-GHz processor and 4-Gbyte RAM memory. The software package is written in C++ language, with a managing control program elaborated with PYTHON that governs the different steps (basis construction, $\mathcal{Q}$ and $\mathcal{P}$ eigenvalue problems, energy shifts computations, inverse interpolation procedure to obtain the Auger widths, graphical interface, etc.) plus the drivers for algebra libraries LAPACK through SciPy [38].

III. RESULTS AND DISCUSSION

In this work we aim to perform systematic computations with the Feshbach formalism for the lowest doubly excited states of the helium atom immersed in a weakly coupled plasma with different screening parameters $\lambda = 1/D$. Information on the evolution of resonance energies and specially their Auger widths is quite scattered in the bibliography and conclusiveness on their behavior against the screening strength is elusive. To our knowledge, this is the first application of the Feshbach formalism to study resonance parameters in atoms embedded in a weakly coupled plasma, using also explicitly correlated coordinates. The latter choice of Slater-type correlated basis avoids the expansion of the screened Coulomb interelectronic interaction $e^{-\lambda r_{12}}/r_{12}$ in terms of $r_>$ and $r_<$ and all integrals are analytical. On the other hand, CI computations in terms of explicitly correlated coordinates have some disadvantages, concerning (i) the omnipresent linear dependencies

TABLE I. Plasma-free computations (with $\lambda = 0$) for energies and widths of He doubly excited states below the He^+ ($N = 2$) threshold, with $^1S^e$, $^1P^o$, and $^1D^e$ symmetries. Present computations are compared with results by Chen [39] (an extended comparison with other computations is included in this reference). Numbers in squared brackets indicate powers of ten.

	$^1S^e$			$^1P^o$			$^1D^e$		
	${}_{n_1}(K,T)^A_{n_2}$	$-E_r$ (a.u.)	Γ (a.u.)	${}_{n_1}(K,T)^A_{n_2}$	$-E_r$ (a.u.)	Γ (a.u.)	${}_{n_1}(K,T)^A_{n_2}$	$-E_r$ (a.u.)	Γ (a.u.)
Present	${}_2(1,0)^+_2$	0.777940	4.60[−3]	${}_2(0,1)^+_2$	0.692927	1.30[−3]	${}_2(1,0)^+_2$	0.702129	2.29[−3]
Ref. [39]		0.77787	4.53[−3]		0.693069	1.372[−3]		0.70183	2.36[−3]
Present	${}_2(-1,0)^+_2$	0.621864	2.43[−4]	${}_2(1,0)^-_3$	0.597074	3.85[−6]	${}_2(1,0)^+_3$	0.569269	5.33[−4]
Ref. [39]		0.62181	2.178[−4]		0.597074	3.84[−6]		0.569193	5.60[−4]
Present	${}_2(1,0)^+_3$	0.589929	1.35[−3]	${}_2(0,1)^+_3$	0.564048	2.85[−4]	${}_2(0,1)^0_3$	0.556431	1.88[−5]
Ref. [39]		0.589896	1.37[−3]		0.564074	2.998[−4]		0.556417	2.01[−5]
Present	${}_2(-1,0)^+_3$	0.548081	8.82[−5]	${}_2(-1,0)^0_3$	0.547070	1.82[−8]	${}_2(1,0)^+_4$	0.536747	2.22[−4]
Ref. [39]		0.548070	7.75[−5]		0.547087	1.5[−8]		0.536715	2.34[−4]
Present	${}_2(1,0)^+_4$	0.544891	4.78[−4]	${}_2(1,0)^-_4$	0.546482	2.02[−6]	${}_2(0,1)^0_4$	0.531513	1.04[−5]
Ref. [39]		0.544882	5.0[−4]		0.546490	2.02[−6]		0.531506	1.12[−5]
Present	${}_2(-1,0)^+_4$	0.527717	5.47[−5]	${}_2(0,1)^+_4$	0.534314	1.22[−4]	${}_2(-1,0)^0_4$	0.529293	1.12[−8]
Ref. [39]		0.527707	4.9[−5]		0.534358	1.28[−4]		0.529292	1.21[−8]
Present	${}_2(1,0)^+_5$	0.526689	2.09[−4]	${}_2(-1,0)^0_4$	0.527573		${}_2(1,0)^+_5$	0.522753	1.11[−4]
Ref. [39]		0.526687	2.3[−4]		0.527613	3[−9]		0.522737	1.18[−4]
Present	${}_2(-1,0)^+_5$	0.518105	3.50[−5]				${}_2(0,1)^0_5$	0.520118	5.93[−6]
Ref. [39]		0.518100	3.2[−5]					0.520114	6.40[−6]
Present	${}_2(1,0)^+_6$	0.517641	1.08[−4]				${}_2(-1,0)^0_5$	0.519001	1.11[−8]
Ref. [39]		0.517641	1.2[−4]					0.519000	
Present	${}_2(-1,0)^+_6$	0.512760	2.25[−5]				${}_2(1,0)^+_6$	0.515460	6.28[−5]
Ref. [39]		0.512762	2.2[−5]					0.515451	6.76[−5]
Present	${}_2(1,0)^+_7$	0.512509	6.29[−5]				${}_2(0,1)^0_6$	0.513953	3.61[−6]
Ref. [39]		0.512514	6.9[−5]					0.513950	3.82[−6]
Present	${}_2(-1,0)^+_7$	0.509469	1.30[−5]				${}_2(-1,0)^0_6$	0.513311	8.83[−9]
Ref. [39]								0.513310	

when saturating the CI basis for convergence (basis parameters must be always judiciously chosen) and (ii) the poor long-range representation of the electronic continuum along with a low density of states in the energy region of interest. In this sense, computations in terms of B splines or discrete variable representation (DVR) basis sets are shown to be far superior to skip these representation difficulties, but in this case all screened Coulomb two-electron integrals must be computed numerically, which increases noticeably the computational effort. Thus, in this work we want to gauge the capability of the Feshbach method together with explicitly correlated coordinates to shed light on the variation of resonance parameters with Yukawa-like screening potentials as a good test case.

First, in order to establish the accuracy of our Feshbach implementation and the proper selection of the correlated basis set, we have computed resonance parameters for the isolated He atom, for the $^{1,3}S^e$, $^{1,3}P^o$, and $^{1,3}D^e$ symmetries. With the basis quoted in Sec. II B we are able to obtain 34 $^1S^e$ and 22 $^3S^e$ resonances, 25 $^1D^e$ and 24 $^3D^e$ resonances, and 11 $^1P^o$ and 12 $^3P^o$ resonant states below the $He^+(N = 2)$ threshold, although we report energies and widths with converged figures for the lowest 12 $^{1,3}S^e$ resonances, the lowest 12 $^{1,3}D^e$ resonances and the lowest 6 in $^{1,3}P^o$ symmetries. In Tables I (singlets) and II (triplets) we compare our results with the accurate ones obtained by Chen [39] using the saddle-point complex rotation method with B-spline functions. In general, the comparison for both energies and widths is very good. Widths for the triplets around 10^{-11} a.u. are very difficult to extract due to their smallness (Chen [39] does not report these values either). It is worth noting that the largest differences in energy appear in the lowest resonances for each symmetry. This may be due to the approximate representation of the $M\mathcal{P}$ Phillips-Kleinman pseudopotential and the chosen basis. The formal equivalence between the $\mathcal{Q}H\mathcal{Q}$ eigenproblem and the $H_{\text{eff}} = H + M\mathcal{P}$ one, is strictly proven for $M \to \infty$. We have used several increasing values of M, and our results are reported using $M = 300$ since larger values may unbalance the Hamiltonian matrix elements entering in the numerical diagonalization. In addition, in the screened case, the approximated (but a rather good approximation) φ^{λ}_{1s} one-parameter wave function used for the $\mathcal{P}$ projector may lead to small differences in the projection for the most compact resonances in the configurational space.

As mentioned above, we find the $^{1,3}P^o$ symmetry much more complicated to compute in terms of finding an optimized basis set exempt from linear dependencies (keeping our calculations in double precision). Nevertheless we are able to extract converged resonance parameters for at least the lowest six resonances, just enough to have representatives for each $(K,T)^A$ series. The comparison of our $^{1,3}P^o$ results with those of Chen [39] is rather good. Incidentally, the saddle-point method used in Ref. [39] is based on a min-max method and the present method is strictly variational either for the total Hamiltonian or the $\mathcal{Q}$-space projected H_{eff}. Anyway, we do not claim that our results are necessarily better, due to the above-mentioned approximation in the diagonalization of

TABLE II. Plasma-free computations (with $\lambda = 0$) for energies and widths of He doubly excited states below the He^+ ($N = 2$) threshold, with $^3S^e$, $^3P^o$, and $^3D^e$ symmetries. Present computations are compared with results by Chen [39] (an extended comparison with other computations is included in this reference). Numbers in squared brackets indicate powers of ten.

	$^3S^e$			$^3P^o$			$^3D^e$		
	${}_{n_1}(K,T)^A_{n_2}$	$-E_r$ (a.u.)	Γ (a.u.)	${}_{n_1}(K,T)^A_{n_2}$	$-E_r$ (a.u.)	Γ (a.u.)	${}_{n_1}(K,T)^A_{n_2}$	$-E_r$ (a.u.)	Γ (a.u.)
Present	${}_2(1,0)^-_3$	0.602576	6.39[−6]	${}_2(1,0)^+_2$	0.760506	3.12[−4]	${}_2(1,0)^-_3$	0.583776	3.06[−8]
Ref. [39]		0.602577	6.65[−6]		0.760489	2.99[−4]		0.583784	3.12[−8]
Present	${}_2(-1,0)^-_3$	0.559744	2.49[−7]	${}_2(1,0)^+_3$	0.584675	8.56[−5]	${}_2(0,1)^0_3$	0.560643	7.20[−6]
Ref. [39]		0.559745	2.61[−7]		0.584671	8.24[−5]		0.560684	7.56[−6]
Present	${}_2(1,0)^-_4$	0.548840	2.96[−6]	${}_2(0,1)^-_3$	0.579028	1.80[−6]	${}_2(1,0)^-_4$	0.541675	1.05[−8]
Ref. [39]		0.548841	3.10[−6]		0.579030	1.85[−6]		0.541679	1.0[−8]
Present	${}_2(-1,0)^-_4$	0.532504	1.37[−7]	${}_2(-1,0)^-_3$	0.548838	2.74[−8]	${}_2(0,1)^0_4$	0.533438	3.66[−6]
Ref. [39]		0.532505	1.43[−7]		0.548841	1.30[−8]		0.533462	3.82[−6]
Present	${}_2(1,0)^-_5$	0.528413	1.47[−6]	${}_2(1,0)^+_4$	0.542834	3.27[−5]	${}_2(-1,0)^0_4$	0.529308	2.48[−11]
Ref. [39]		0.528414	1.54[−6]		0.542837	3.17[−5]		0.529312	7[−11]
Present	${}_2(-1,0)^-_5$	0.520548	7.85[−8]	${}_2(0,1)^-_4$	0.539532	7.91[−7]	${}_2(1,0)^-_5$	0.525016	4.47[−9]
Ref. [39]		0.520549	8.2[−8]		0.539558	7.90[−7]		0.525018	4.8[−9]
Present	${}_2(1,0)^-_6$	0.518541	8.15[−7]	${}_2(-1,0)^-_4$	0.528165		${}_2(0,1)^0_5$	0.521109	1.97[−6]
Ref. [39]		0.518546	8.6[−7]		0.528637	6.6[−9]		0.521130	2.08[−6]
Present	${}_2(-1,0)^-_6$	0.514173	4.85[−8]				${}_2(-1,0)^0_5$	0.518996	∼[11]
Ref. [39]		0.514180	4.8[−8]					0.519016	
Present	${}_2(1,0)^-_7$	0.513021	5.03[−7]				${}_2(1,0)^-_6$	0.516686	2.33[−9]
Ref. [39]		0.513046	5.2[−7]					0.516687	2.5[−9]
Present	${}_2(-1,0)^-_7$	0.510311	3.75[−8]				${}_2(0,1)^0_6$	0.514520	1.17[−6]
Ref. [39]		0.510378	3.0[−8]					0.514540	1.2[−6]
Present	${}_2(1,0)^-_8$	0.509586	3.44[−7]				${}_2(-1,0)^0_6$	0.513278	∼[11]
Ref. [39]								0.513322	
Present	${}_2(-1,0)^-_8$	0.507469					${}_2(1,0)^-_7$	0.511919	1.12[−9]

the effective Hamiltonian H_{eff} and the difficulties to saturate the configurational space with a correlated basis. However, our main concern is to work with a basis of configurations good enough to subsequently provide reliable results for the screened case. At this point, we should mention that we have not made an attempt to vary or optimize the basis of correlated configurations for every single value of λ and the same basis for $\lambda = 0$ is then used for all calculations presented in this work. This may imply eventually that the *virtual* representation of the energy positions of $He^+(2s,2p) + e^-$ thresholds may be slightly misplaced in the two-electron calculation, when compared to the one-particle energies $He^+(2s)$ and $He^+(2p)$, computed separately with much higher precision.

Once our correlated basis set and Feshbach procedure is reasonably tested for $\lambda = 0$, we proceed to perform systematic calculations for energies and widths for the lowest singlet and triplet resonances located below the $He^+(N = 2)$ threshold. The leading order in λ for the screened potential in the last row of Eq. (1) [it follows from $V(r_1,r_2,r_{12}) = -\frac{Z}{r_1} - \frac{Z}{r_2} + \frac{1}{r_{12}} + \lambda(2Z-1) + \cdots$] clearly shows that the screening is an effective repulsive interaction, so that energies must increase their value (they become less bound) for increasing λ. According to this simple formula, the states in He increase their energies faster than the one-electron states of the parent ion He^+, which implies that the energies for bound and quasibound (resonant) states eventually cross the upper ionic thresholds for some critical values of the screening parameter λ. This behavior for the resonance energies is represented in the top part of plots from Figs. 1 to 6, where for the sake of clarity we choose to represent the energy difference from the upper $He^+(2s)$ threshold. Here, the values for the threshold energies $He^+(2s)$ and $He^+(2p)$ are obtained by diagonalizing the plasma-embedded He^+ Hamiltonian in a variational basis set of Slater-type orbitals, which compare well with the values reported in Ref. [16]. We show the variation of resonance energies and widths against the screening parameter, i.e., (E_r,Γ_r) vs λ, in graphical form instead of voluminous tabular data, which are available from the authors upon request [40]. Nevertheless, to assess the quality and accuracy of our numerical data we choose to compare in Table III our results for the lowest singlet resonances ($^1S^e$, $^1P^o$, and $^1D^e$) with those reported by Ho *et al.* [14,16,17,23], using the stabilization method. Due to the effectiveness of our computational method, we can provide values for higher resonances and for a much finer mesh of λ values, including also the values for λ used by Ho *et al.* for the sake of comparison. Accordingly, we also include in our figures the results reported by Ho *et al.* for some states and symmetries, when available. The comparison is remarkably good [though with noticeable small differences for the widths of the $^{1,3}D^e$ ${}_2(0,1)^0_4$ states] for energies and especially for the widths, which are more affected by the quality of the wave functions.

In the latter works Ho *et al.* use the stabilization method in which the nonlinear parameters in the basis may be chosen so that the energy of the lowest bound state is a minimum for each value of λ. Resonances are instead high-lying excited

TABLE III. Resonance energies and widths for the first lowest $^1S^e$, $^1P^o$, and $^1D^e$ doubly excited states below the second ionization threshold $He^+(N = 2)$ of plasma embedded He for a sequence of screening parameters $\lambda \in [0,1/3]$ (or corresponding Debye lengths $D = 1/\lambda$). Present calculations are compared with data available from different works by Kar and Ho using the stabilization method in Refs. [14,16,17,23]. Numbers in squared brackets indicate powers of ten.

		$^1S^e$ $[_2(1,0)_2^+]$		$^1P^o$ $[_2(0,1)_2^+]$		$^1D^e$ $[_2(1,0)_2^+]$	
$\lambda = 1/D$ (a.u.)		$-E_r$ (a.u.)	Γ (a.u.)	$-E_r$ (a.u.)	Γ (a.u.)	$-E_r$ (a.u.)	Γ (a.u.)
$1/\infty$	Present	0.77794	4.60[−3]	0.692927	1.30[−3]	0.70213	2.29[−3]
	Kar and Ho	0.77783	4.549[−3]	0.69313	1.377[−3]	0.7019477	2.376[−3]
1/100	Present	0.74831	4.59[−3]	0.66336	1.30[−3]	0.67251	2.28[−3]
	Kar and Ho	0.74819	4.545[−3]	0.66355	1.376[−3]	0.6723257	2.372[−3]
1/70	Present	0.73584	4.58[−3]	0.65094	1.30[−3]	0.66004	2.27[−3]
	Kar and Ho	0.73572	4.540[−3]				
1/50	Present	0.71941	4.56[−3]	0.63463	1.29[−3]	0.64363	2.27[−3]
	Kar and Ho	0.71929	4.533[−3]	0.63482	1.369[−3]	0.6434478	2.362[−3]
1/40	Present	0.70523	4.55[−3]	0.62057	1.29[−3]	0.62947	2.26[−3]
	Kar and Ho	0.70513	4.531[−3]				
1/30	Present	0.68198	4.52[−3]	0.59757	1.28[−3]	0.60626	2.24[−3]
	Kar and Ho	0.68188	4.496[−3]	0.59777	1.354[−3]	0.6060725	2.338[−3]
1/20	Present	0.63694	4.45[−3]	0.55321	1.27[−3]	0.56130	2.19[−3]
	Kar and Ho	0.63683	4.450[−3]	0.55340	1.327[−3]	0.5611172	2.294[−3]
1/15	Present	0.59377	4.36[−3]	0.51096	1.22[−3]	0.51825	2.13[−3]
	Kar and Ho			0.51113	1.296[−3]	0.5180639	2.234[−3]
1/12	Present	0.55245	4.25[−3]	0.47069	1.18[−3]	0.47704	2.05[−3]
	Kar and Ho					0.4768582	2.161[−3]
1/10	Present	0.51291	4.13[−3]	0.43232	1.13[−3]	0.43763	1.97[−3]
	Kar and Ho	0.51279	4.159[−3]	0.43252	1.197[−3]	0.4374521	2.076[−3]
1/8	Present	0.45687	3.92[−3]	0.37829	1.05[−3]	0.38179	1.82[−3]
	Kar and Ho			0.37851	1.109[−3]	0.3816262	1.931[−3]
1/7	Present	0.41919	3.75[−3]	0.34219	9.79[−4]	0.34426	1.71[−3]
	Kar and Ho	0.41906	3.794[−3]				
1/6	Present	0.37188	3.50[−3]	0.29722	8.85[−4]	0.29720	1.54[−3]
	Kar and Ho			0.29741	9.41[−4]	0.2970523	1.644[−3]
1/5	Present	0.31114	3.13[−3]	0.23997	7.45[−4]	0.23690	1.30[−3]
	Kar and Ho	0.31105	3.191[−3]	0.24016	7.91[−4]	0.2367763	1.388[−3]
1/4	Present	0.23158	2.53[−3]	0.16631	5.22[−4]	0.15845	9.17[−4]
	Kar and Ho	0.23151	2.591[−3]	0.16649	5.5[−4]	0.158376	9.86[−4]
1/3	Present	0.12798	1.52[−3]	0.084924		0.085612	1.31[−10]
	Kar and Ho	0.12792	1.569[−3]				

states immersed in a discretized pseudocontinuum within the same full diagonalization. An optimized basis for the ground state may induce a much-too-compact representation of the resonant wave functions. Consequently, a basis set very well adapted to compute bound states may provide instead a poorer representation of the diffuseness linked to doubly excited states. In our Feshbach method, resonances are instead the lowest states in the $\mathcal{Q}H\mathcal{Q}$ eigenvalue problem. Then a subtle compromise must be met to find the adequate basis parameters better adapted to our Feshbach $\mathcal{Q}H\mathcal{Q}$ eigenvalue problem.

Our main concern here is the systematic behavior of the resonance widths (Auger lifetimes) against the increasing λ parameter, which indicates the robustness of their survival in a plasma environment. We find that the general behavior for the widths follows a similar pattern for those resonances classified within the same series of $(K,T)^A$ numbers under the same L, S, and π symmetries. For $L = 0$ states, there are only two $(K,T)^A$ series for both $^1S^e$ and $^3S^e$ symmetries, $_2(1,0)_n^+$ and $_2(-1,0)_n^+$ for the singlets and $_2(1,0)_n^-$ and $_2(-1,0)_n^-$ for the triplets. In Fig. 1 we plot the widths for the lowest 12 $^1S^e$ resonances, 6 resonances within the $_2(1,0)_n^+$ series, and 6 resonances within the $_2(-1,0)_n^+$ series, with $N = 2$ and n varying from 2 to 7. We have made computations for a dense grid of λ values up to $\lambda = 0.35$ and only the lowest resonance crosses the upper threshold beyond that value (not shown in the figure). It is noticeable that resonances within the same series show a similar behavior against the variation with λ. Those in the $_2(1,0)_n^+$ series decrease monotonically their widths as λ increases. At variance, the resonances in the $_2(-1,0)_n^+$ series increase their widths to reach a maximum before the critical value of λ at which the resonance crosses the $He^+(2s)$ threshold and then decrease abruptly in the neighborhood of the threshold. A similar behavior is found in Fig. 2 for the triplets, which share the same (K,T) numbers but differ in the A label ($+$ for the singlets and $-$ for the triplets). Note that in the $^3S^e$ the behavior of the state $_2(-1,0)_7^-$ departs from the precedent states in the same series, and its width always decreases for increasing λ. This may be due

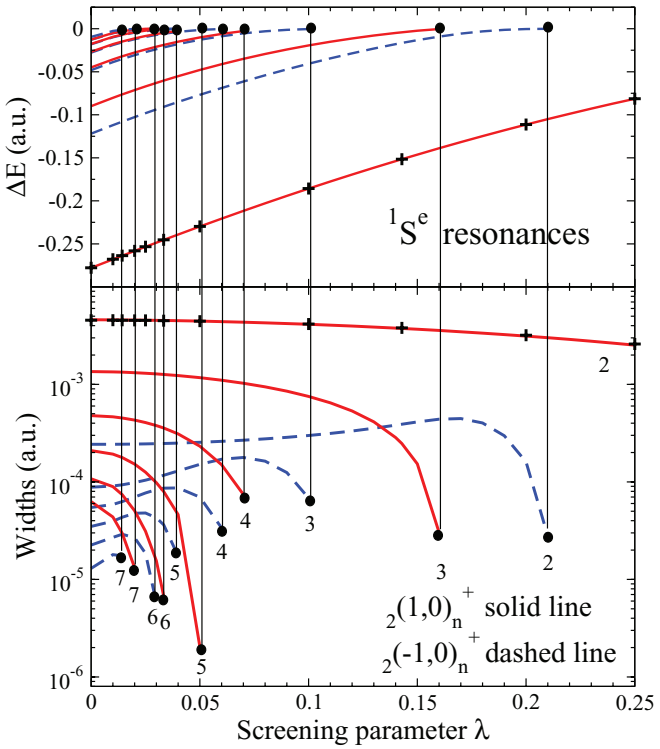

FIG. 1. (Color online) (Top) Plot of $\Delta E = E - E_{\rm Th}$ [energy difference between those of the twelve lowest He $^1S^e$ doubly excited states and the upper $He^+(2s)$ threshold energy] against the screening parameter λ. The dot indicates the critical value of λ at which each Feshbach resonance reaches the threshold (i.e., $\Delta E = 0$). Six $^1S^e$ resonances pertaining to the $_2(1,0)_n^+$ series are plotted with solid lines and those 6 of the $_2(-1,0)_n^+$ series with dashed lines. (Bottom) Evolution of the resonance widths for the lowest 12 He $^1S^e$ doubly excited states below the $He^+(2s)$ threshold as a function of the screening parameter λ. The same scheme of colors and lines used for the resonance energies is employed for the widths. The largest width within a series correspond to the lowest values of n in $_2(K,T)_n^A$ for $\lambda = 0$. Vertical lines connect energies and widths at the critical λ value for which the widths can be computed below the $He^+(2s)$ threshold. Numerical labels in the widths indicate the excitation index n that identifies each resonance. The symbols + indicate the values calculated with the stabilization method reported in Ref. [14].

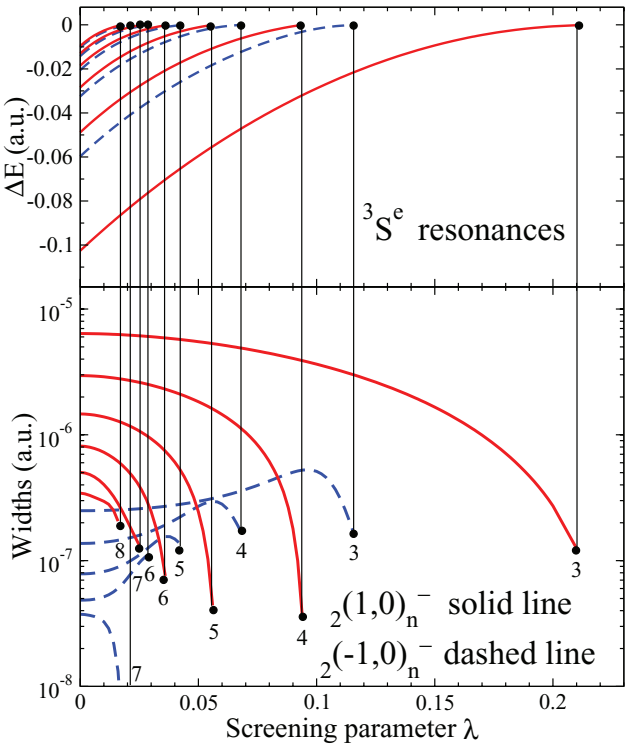

FIG. 2. (Color online) (Top) The same as in Fig. 1 (top) but for the lowest 11 He $^3S^e$ resonances. Here, the first 6 resonances from the $_2(1,0)_n^-$ series are plotted with solid lines and the first 5 resonances within the $_2(-1,0)_n^-$ series with dashed lines. (Bottom) Same as in Fig. 1 for the widths.

to the closer proximity of the upper threshold. Unfortunately, we cannot infer whether this decreasing behavior follows for higher resonances $_2(-1,0)_{n>7}^-$ at small values of λ since the calculation of widths is not numerically reliable.

The behavior of resonance widths against increasing λ has been analyzed in the past by Ho *et al.* [19,22] in terms of the different geometrical arrangement adopted by the two electrons with respect to the nucleus in "+" and "–" states, which refer to the Cooper-Fano-Pratts classification of resonance series [41], or to the A values ±1, respectively, in the Lin classification [10]. The explanation given by Ho follows the following reasoning. In the "+" states [with antinodal behavior at $r_1 = r_2$ in the two-electron radial density $\rho(r_1,r_2)$] the two electrons are located on opposite sides of the nuclei and they move "in phase" (anticorrelated motion) toward the nucleus. Autoionization proceeds when one of the electrons is "knocked out" by the other via the nucleus. Then the effect of screening is to slow down the stretching motion of both electrons, the lifetime being then prolonged and the width is smaller when the screening increases. In the "−" states (with a nodal behavior at $r_1 = r_2$ in the two-electron radial density) the most probable radial geometry implies that one of the electrons remains closer to the nucleus than the other. The outer electron feels the (He^+,e^-) pair through a charge plus dipole potential, whose strength diminishes as the screening increases, leading to a more rapid autoionization of the outer electron; i.e., the width tends to increase its value. According to our calculations (even only for the $L = 0$ states), we find this explanation not general. Indeed, the behavior of the widths in this case seems to be mostly ruled by the angular correlation given by the label K; i.e., the widths decrease their value for $K = +1$ and increase for $K = -1$, without an explicit role played by the radial correlation number $A = \pm 1$.

However, this dependence on the K number for the $L = 0$ states is no longer fully supported for resonance states with $L = 1$ (singlets and triplets). In Figs. 3 and 4 we include the variation of resonance energies and widths against the screening parameter λ. Energies and widths are plotted up to the value of λ at which each resonance energy crosses the upper $He^+(2s)$ threshold. The resonant states in the series $_2(0,1)_n^+$ for the $^1P^o$ and in the series $_2(1,0)_n^+$ for the $^3P^o$ reduce their widths monotonically with respect to λ (the plasma screening increase their lifetime). These two series showing similar behavior have different angular correlation numbers (K,T) but the same radial correlation pseudoquantum number $A = +1$. The next series is $_2(1,0)_n^-$ for $^1P^o$ and $_2(0,1)_n^-$ for $^3P^o$, again

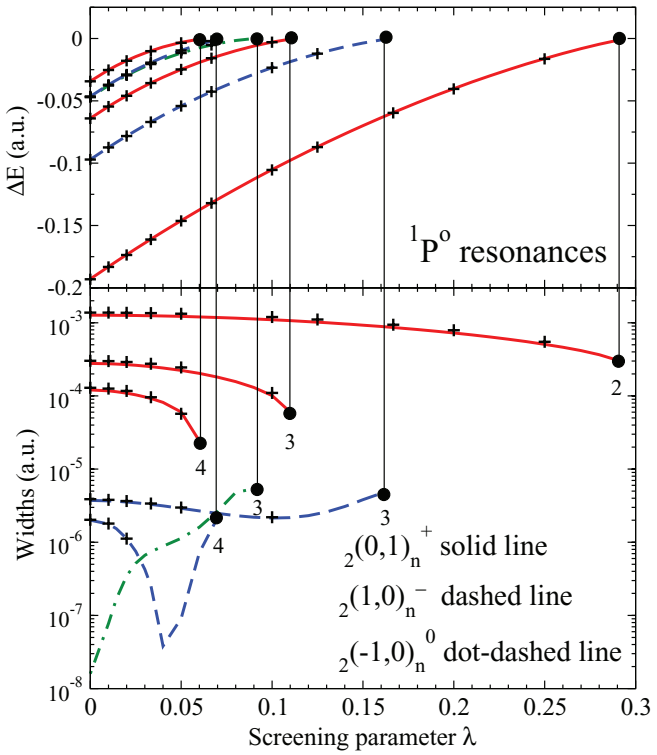

FIG. 3. (Color online) (Top) The same as in Fig. 1 (top) but for the lowest six He $^1P^o$ resonances. Here, three resonances from the $_2(0,1)_n^+$ series are plotted with solid lines; two resonances from the $_2(1,0)_n^-$ series with dashed lines and the resonance $_2(-1,0)_3^0$ with dot-dashed line. (Bottom) Same as in Fig. 1 for the widths. The symbols + indicate the values calculated with the stabilization method reported in Ref. [17].

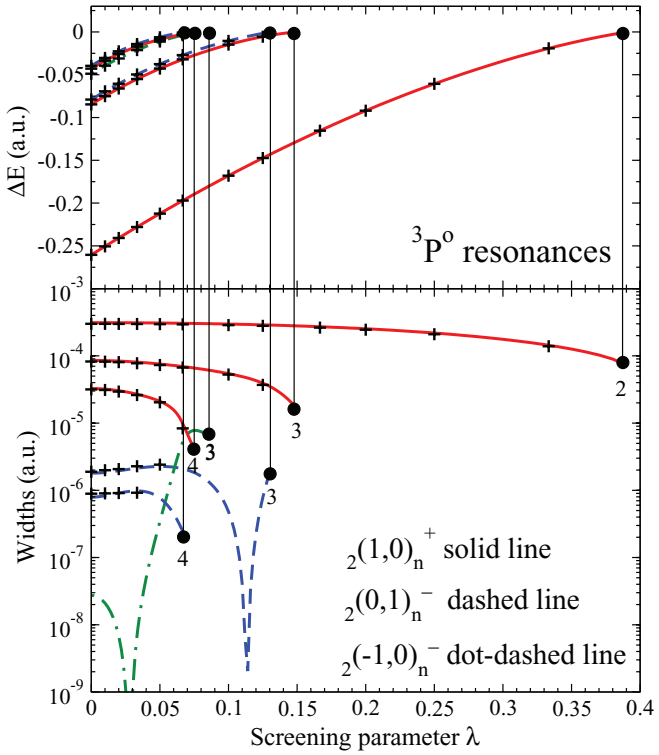

FIG. 4. (Color online) (Top) The same as in Fig. 1 (top) but for the lowest six He $^3P^o$ resonances. Here, three resonances from the $_2(1,0)_n^+$ series are plotted with solid lines, two resonances from the $_2(0,1)_n^-$ series with dashed lines, and the resonance $_2(-1,0)_3^-$ with dot-dashed line. (Bottom) Same as in Fig. 1 for the widths. The symbols + indicate the values calculated with the stabilization method reported in Ref. [17].

with different (K,T) numbers but the same number $A=-1$. In spite of this, their tendency against λ is different: The former series in the singlets first decrease for small λ values, then increasing for larger values, and the latter in the triplets show the opposite behavior, they slightly increase to finally decrease abruptly before crossing the threshold. Incidentally, the sudden increase of the $_2(0,1)_3^-$ $^3P^o$ after the sharp minimum in the widths before reaching the $He^+(2s)$ threshold may be due to the shifted position of this threshold in the two-electron calculation against the energy obtained in the one-electron calculation for the $He^+(2s)$ state in the one-electron Yukawa potential (which is much more accurate than the two-electron calculation in that energy region). Most probably, the minimum in the width in Fig. 4 at $\lambda=0.112$ for the $_2(0,1)_3^-$ $^3P^o$ corresponds to the threshold crossing in the two-electron calculation, and the sudden increase can be attributed to its behavior after the crossing (a region in which the Feshbach partitioning is no longer valid). We further comment on this issue below, regarding the conversion of the Feshbach resonances below the threshold into shape resonances above it. Intuitively, a shape resonance confined by a potential should increase its width as the screening augments, since the height of the barrier reduces its value when the energy increases, leading to a shorter lifetime [9]. Finally, the only representative in the series $_2(-1,0)_n^0$ for the singlet $^1P^o$ and $_2(-1,0)_n^-$ for the triplet $^3P^o$ share the same (K,T) numbers but different A number (0 and −1, respectively) and they have the most dramatic changes in the widths, mostly increasing their value by orders of magnitude. In this case, in contrast to the above-mentioned $_2(0,1)_3^-$ $^3P^o$ resonance, the sharp minimum in the width located at $\lambda=0.028$ for the $_2(-1,0)_3^-$ $^3P^o$ resonance cannot be attributable to the threshold crossing (it is still quite far from the threshold position) and it might be due to a sudden transformation of the resonant wave function at this value of λ.

Finally, the energies and widths for $L=2$ are included in Fig. 5 for the $^1D^e$ and Fig. 6 for the $^3D^e$. The Rydberg series of resonances for the $^3D^e$ lie much closer to the $He^+(N=2)$ threshold in comparison to the other symmetries, so that for a screening parameter $\lambda\sim 0.13$ all resonances have already crossed the upper $He^+(2s)$ threshold. The series with the largest widths in the figures [note here that the lowest $^3D^e$ resonance $_2(1,0)_3^-$ does not have the largest width for $\lambda=0$, and this symmetry then represents a peculiar case in He], i.e., $_2(1,0)_n^+$ for the singlets (solid lines) and $_2(0,1)_n^0$ for the triplets (dashed lines) show a similar smooth decreasing trend for the widths against λ. One may even compare the widths for the $_2(0,1)_n^0$ $^1D^e$ (dashed lines) and the $_2(1,0)_n^-$ $^3D^e$ (solid lines) series and conclude that for small values of λ their behavior is analogous, to strongly depart for larger values. Finally, the series starting with the smallest widths for $\lambda=0$, $_2(-1,0)_n^0$ $^1D^e$, and $_2(-1,0)_n^0$ $^3D^e$ (dot-dashed lines in both

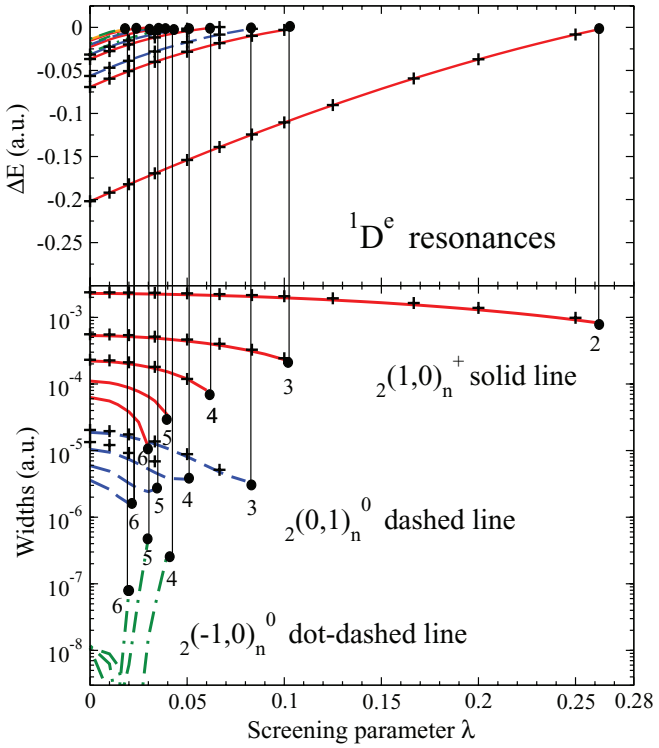

FIG. 5. (Color online) (Top) The same as in Fig. 1 (top) but for the lowest 12 He $^1D^e$ resonances. Here, 5 resonances from the $_2(1,0)_n^+$ series are plotted with solid lines, 4 resonances from the $_2(0,1)_n^0$ series with dashed lines, and 3 resonances from the $_2(-1,0)_n^0$ series with dot-dashed line. (Bottom) Same as in Fig. 1 for the widths. The symbols + indicate the values calculated with the stabilization method reported in Ref. [23].

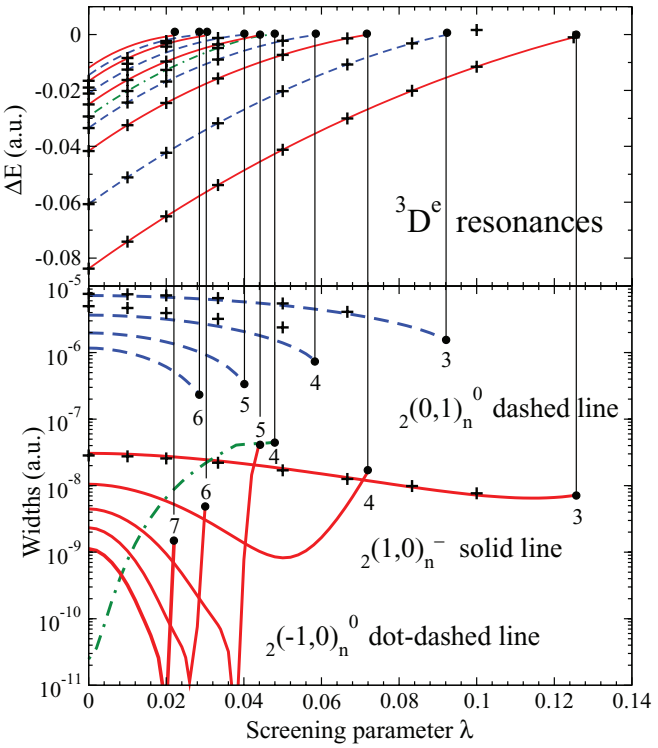

FIG. 6. (Color online) (Top) The same as in Fig. 1 (top) but for the lowest ten He $^3D^e$ resonances. Here, five resonances from the $_2(1,0)_n^-$ series are plotted with solid lines, four resonances from the $_2(0,1)_n^0$ series with dashed lines, and one resonance from the $_2(-1,0)_n^0$ series with a dot-dashed line. (Bottom) Same as in Fig. 1 for the widths. The symbols + indicate the values calculated with the stabilization method reported in Ref. [23].

cases) have a different behavior against λ in spite of sharing the same $(K,T)^A$ numbers. However, their tendency is to reduce their lifetimes (increase their widths) by several orders of magnitude, similar to the trend of the series $_2(-1,0)_n^-$ $^3P^o$ and $_2(-1,0)_n^0$ $^1P^o$ (dot-dashed lines in Figs. 4 and 3), respectively.

Some of these partial analogies could indicate a sort of equivalence in terms of the isomorphic series (those states having identical $(K,T)^A$ numbers [42]) but, in general, we have shown from *ab initio* calculations that this variety of behaviors of the widths seems to preclude clear propensity rules in terms of the $(K,T)^A$ labels alone (referred to $\lambda = 0$), with no regard for the L, S, and π labels, to elucidate the stability of resonances against the variation of the plasma screening. This may indicate a noticeable breakup of the degeneracy associated to the isomorphic *molecular* curves in hyperspherical coordinates [42] and therefore different transformations of the resonance wave functions when augmenting the screening strength. Then we have computed the averaged interelectronic angle for each resonance [in this case $\langle\cos\theta_{12}\rangle$, which can be performed readily with correlated configurations since $\cos\theta_{12} = (r_1^2 + r_2^2 - r_{12}^2)/2r_1r_2$]. For instance, in Fig. 7 we include the variation of the interelectronic angle with the screening parameter for the singlet resonances with labels $_N(K,T)_n^A$ (at $\lambda = 0$). The angular electronic correlation is given by the label K, in such a way that it gives the leading order for the averaged cosine of the interelectronic angle, i.e., $\langle\cos\theta_{12}\rangle \sim -K/N$ and it may be regarded as a bending vibrational quantum number in the *molecular* arrangement $(e^-, \mathrm{He}^{2+}, e^-)$. For $^1S^e$, it is clear from Fig. 7 that resonances within the series $_2(1,0)_n^+$, with $K = +1$, have two electrons mostly located on opposite sides of the nucleus, whereas resonances in the $_2(-1,0)_n^+$ series with $K = -1$ have the electron pair located on the same side of the nucleus. These structures are well established for $\lambda = 0$. From the latter figure we learn that the molecular structure of the lowest resonances within each series is more robust against the variation of λ, only to change abruptly when approaching the crossing with the upper threshold, a limit in which the average angle tends to 90°, indicating that in the electronic continuum above the threshold the electron correlation is mostly lost and the averaged angle representing this situation is any angle between 0° and 180°, i.e., 90°. The proximity of the upper $\mathrm{He}^+(2s)$ threshold for the higher resonances makes them to rapidly change their geometry against the variation of λ. An explanatory remark here is mandatory. Strictly speaking, within the Feshbach method, we can follow the behavior of Feshbach resonances in He only as long as they lie below the ionization threshold. Due to our explicit $\mathcal{Q}-\mathcal{P}$ partitioning, the $\mathcal{Q}$ space does not only contain a pure resonant space due to doubly excited states. In $\mathcal{Q}$ half space remains everything that does not belong to the $(1s,n\ell)$ and $(1s,\epsilon\ell)$ configurations of our $\mathcal{P}$ space. Consequently, the continua $(2s,\epsilon\ell)$ and $(2p,\epsilon\ell)$ are also represented by the $\mathcal{Q}$ configurations and incidentally the Feshbach resonances mix up with the latter continuum

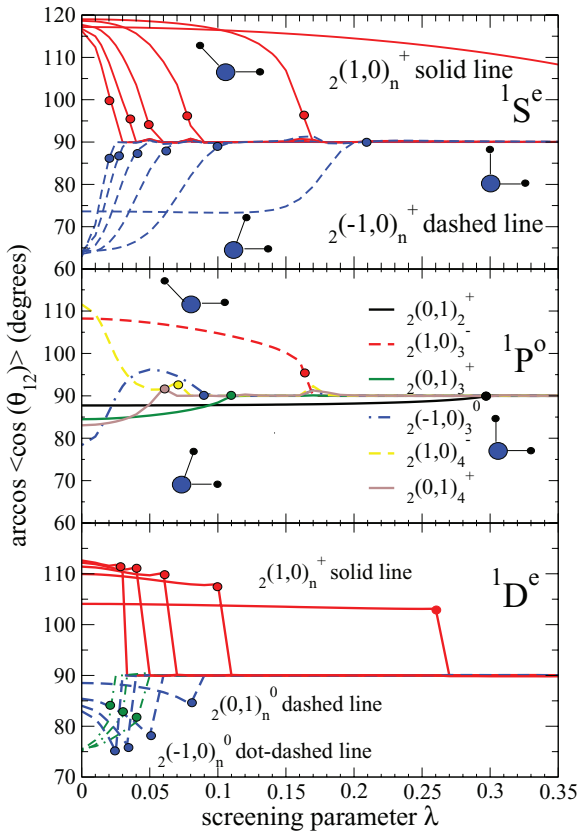

FIG. 7. (Color online) Evolution of the average mean interelectronic angle (calculated as $\cos^{-1}[\langle\cos\theta_{12}\rangle]$) for the resonant states $^1S^e$, $^1P^o$, and $^1D^e$ as a function of the screening parameter λ. The same scheme of colors and lines used in Fig. 1 ($^1S^e$), 3 ($^1P^o$), and 5 ($^1D^e$) is employed here. *Quasimolecular* pictures of the angular geometry of two electrons bound to the nucleus are included to indicate regions with $\theta_{12} > 90°$, $<90°$, or $\sim 90°$. The thick dots on top of the lines indicate the values of λ at which the resonance states cross the upper $He^+(2s)$ threshold.

states once they cross the corresponding thresholds since they become open channels. This limitation in the Feshbach method does not allow us to keep track of individual resonances across thresholds in a smooth topological way.

In the $^1P^o$ symmetry, the resonances in the first series $_2(0,1)^+_{n=2,3,4}$ show a more stable geometrical structure, varying its interelectronic angle smoothly with respect to λ, in agreement with the smooth variation of the widths in Fig. 3. At variance, although the lowest resonance in the series $_2(1,0)^-_n$ has a smooth variation, the second one, $_2(1,0)^-_4$, changes its angular structure more abruptly against λ in the interval [0,0.07], which partially explains the irregular behavior of its width in Fig. 3. The most dramatic behavior in the symmetry $^1P^o$ corresponds to the $_2(-1,0)^0_3$ resonance, with a rapidly increasing width against λ. This value for the width must be accompanied by a more abrupt rearrangement in the electronic structure of the resonance wave function. In fact, the averaged interelectronic angle in Fig. 7 has an oscillating behavior as a function of λ before crossing the threshold.

In the $^1D^e$ symmetry, the resonances in the first and second series, $_2(1,0)^+_n$ and $_2(0,1)^0_n$ have a smooth variation of widths. Noticeably, the angular geometry (see Fig. 7) for the former series $_2(1,0)^+_n$ barely changes against λ, to change abruptly only in the close vicinity of the He^+ $(2s)$ threshold. At variance with the other series in the singlets, that in general approach the angle 90° monotonically, the $_2(0,1)^0_n$ series separates from 90°, reducing their angle, to finally collapse to 90° in a sudden manner close to the threshold crossing. Finally, the $_2(-1,0)^0_n$ series increases the interelectronic angle monotonically against λ, in spite of the irregular behavior of the widths shown in Fig. 5, indicating that in some series the radial correlation rearrangement may dominate over the angular correlations. Plots of the two-particle radial density $\rho(r_1,r_2)$ are more involved to obtain using computational schemes with correlated coordinates containing terms with r_{12} than with uncorrelated configuration interaction wave functions, and we have not built up the two-particle radial density distributions as a function of λ, which eventually could indicate the change in the radial correlations with the screening strength. Anyway, this work indicates that resonance wave functions ultimately may transform in different ways (both radial and angular correlations) as a function of the screening according to the $(K,T)^A$ series. Some series and some resonances within the same series show more robustness in their electronic structure against the screening than others. However, in general, no general trend [according to isomorphic groups sharing the same $(K,T)^A$ labels] can be extrapolated from the resonance classification valid for $\lambda = 0$.

IV. CONCLUSIONS AND PERSPECTIVES

In this paper we have implemented a Feshbach formalism within a configuration interaction method based on explicitly correlated configurations to study the variation of resonance parameters (energy positions and widths) of doubly excited states in plasma-embedded He as a function of the screening parameter in the Debye-Hückel model of the plasma. The method here proposed is accurate and more efficient computationally than other methods previously adapted to this kind of plasma studies, like the stabilization method. To illustrate the fine working of our methodology, we have comprehensively computed and compiled in this work the resonance parameters for many He $^{1,3}S^e$, $^{1,3}P^o$, and $^{1,3}D^e$ doubly excited states, located below the second ionization threshold $He^+(N = 2)$ in the unscreened He, and their evolution against the variation of the screening parameter. Our results for the unscreened case are given in the form of tables to compare with many existing data. For the screened case, we provide in tabular form resonance parameters for the lowest resonance in the singlets ($^1S^e$, $^1P^o$, and $^1D^e$ for an assortment of Debye lengths), for which some previous data are available to compare with. Our main results are given in graphical form, from Figs. 1 to 6, which include energies and widths for the resonant states against the screening parameter before crossing the upper $He^+(2s)$ threshold.

Our study with the Feshbach method cannot disentangle the behavior of the Feshbach resonances once they cross the $He^+(2s,2p)$ thresholds when embedded in a plasma. A resonance state with energy value located above the $He^+(2s,2p)$ thresholds may manifest itself as a shape resonance. This crossover of Feshbach resonances to shape resonances has

already been pointed out in Ref. [43] by analyzing the effect of the Coulomb screening in electron-hydrogen scattering around the $N = 2$ threshold, using the R-matrix method and fitting the eigenphase sum in the vicinity of the threshold. Their widths show a steady decreasing trend for small values of λ, they fall very rapidly before crossing the lowest threshold $H(2s)$, then increasing abruptly after the crossover as expected for shape resonances. These results have been more recently questioned by a recent work by Ho and Kar [44], who have used here the complex scaling method and reported discrepancies in the behavior of the $2s3s\ ^1S^e$ resonance in H^- (quoted $^1S^e(2)$ in Ref. [43]). Most probably, the implementation of the complex scaling with larger basis sets may shed more light to this particular question in a more quantitative way. In fact, we have also used the complex scaling (CS) method during the proceedings of this work, using the same correlated basis. Again, all integrals appearing in the complex rotation procedure can be arranged in closed form and CS calculations may be performed straightforwardly. Nevertheless, our CS calculations in terms of our finite basis of correlated Slater-type orbitals do not provide enough density of states in the vicinity of the two involved thresholds (complex values in the continuum branch) to clearly visualize that sharp Feshbach resonances approaching the continuum as λ increases eventually emerge as shape resonances between the two continuum branches $He^+(2s)$ and $He^+(2p)$ or above $He^+(2p)$. To increase notably such continuum density in the complex plane in that energy region is cumbersome with correlated configurations and one must resort to piecewise basis like B splines or DVR sets. Steps along these lines are under consideration in our group.

ACKNOWLEDGMENTS

We acknowledge financial support by Vicerrectoría de Investigación (Programa Joven Investigador, CODI Menor Cuantía and Estrategia de Sostenibilidad 2013-2014) at Universidad de Antioquia. We also thank F. Martín and Luca Argenti for helpful discussions.

[1] S. Ichimaru, *Plasma Physics: An Introduction to Statistical Physics of Charged Particles* (Benjamin/Cummings, Menlo Park, CA, 1986).
[2] P. Debye and E. Hückel, Phys. Z. **24**, 185 (1923).
[3] A. N. Sil, J. Anton, S. Fritzsche, P. K. Mukherjee, and B. Fricke, Eur. Phys. J. D **55**, 645 (2009).
[4] F. J. Rogers, Phys. Rev. A **10**, 2441 (1974).
[5] C. S. Lam and Y. P. Varshni, Phys. Rev. A **27**, 418 (1983).
[6] S. Kar and Y. K. Ho, Int. J. Quantum Chem. **106**, 814 (2006).
[7] P. Winkler, Phys. Rev. E **53**, 5517 (1996).
[8] F. Brau and F. Calogero, J. Math. Phys. **44**, 1554 (2003).
[9] M. Bylicki, A. Stachów, J. Karwowski, and P. K. Mukherjee, Chem. Phys. **331**, 346 (2007).
[10] C. D. Lin, Phys. Rev. Lett. **51**, 1348 (1983).
[11] D. R. Herrick and O. Sinanoğlu, Phys. Rev. A **11**, 97 (1975).
[12] S. Kar and Y. K. Ho, Phys. Rev. E **70**, 066411 (2004).
[13] S. Kar and Y. K. Ho, New J. Phys. **7**, 141 (2005).
[14] S. Kar and Y. K. Ho, Chem. Phys. Lett. **402**, 544 (2005).
[15] S. Kar and Y. K. Ho, Phys. Rev. A **71**, 052503 (2005).
[16] S. Kar and Y. K. Ho, Phys. Rev. A **72**, 010703(R) (2005).
[17] S. Kar and Y. K. Ho, J. Phys. B: At., Mol. Opt. Phys. **39**, 2445 (2006).
[18] S. Kar and Y. K. Ho, Few-Body Syst. **40**, 13 (2006).
[19] S. Kar and Y. K. Ho, Phys. Rev. A **73**, 032502 (2006).
[20] S. Kar and Y. K. Ho, Int. J. Quantum Chem. **107**, 353 (2007).
[21] S. Kar and Y. K. Ho, Eur. Phys. J. D **44**, 1 (2007).
[22] S. Kar and Y. K. Ho, J. Phys. B: At., Mol. Opt. Phys. **42**, 044007 (2009).
[23] S. Kar and Y. K. Ho, Int. J. Quantum Chem. **110**, 993 (2010).
[24] A. U. Hazi and H. S. Taylor, Phys. Rev. A **1**, 1109 (1970); V. A. Mandelshtam, T. R. Ravuri, and H. S. Taylor, Phys. Rev. Lett. **70**, 1932 (1993).
[25] J. C. Cardona and J. L. Sanz-Vicario, J. Phys. B: At., Mol. Opt. Phys. **41**, 055003 (2008).
[26] H. Feshbach, Ann. Phys. (NY) **19**, 287 (1962).
[27] A. Temkin and A. K. Bhatia, in *Autoionization: Recent Developments and Applications*, edited by A. Temkin (Plenum, New York, 1985), p. 1.
[28] A. Temkin and A. K. Bhatia, Phys. Rev. A **31**, 1259 (1985).
[29] J. C. Cardona, J. L. Sanz-Vicario, and F. Martín, Phys. Rev. A **82**, 022501 (2010).
[30] J. L. Sanz-Vicario, H. Bachau, and F. Martín, Phys. Rev. A **73**, 033410 (2006).
[31] C. M. Granados-Castro and J. L. Sanz-Vicario, J. Phys. B: At., Mol. Opt. Phys. **46**, 055601 (2012).
[32] A. Macías, F. Martín, A. Riera, and M. Yáñez, Phys. Rev. A **36**, 4179 (1987).
[33] F. Martín, O. Mó, A. Riera, and M. Yánez, Europhys. Lett. **4**, 799 (1987).
[34] R. J. Tweed, J. Phys. B: At., Mol. Phys. **5**, 810 (1972).
[35] J. L. Calais and P.-O. Löwdin, J. Mol. Spectrosc. **8**, 203 (1962).
[36] E. Ley-Koo, C. F. Bunge, and R. Jáuregui, Int. J. Quantum Chem. **63**, 93 (1997).
[37] S.-T. Dai, A. Solovyova, and P. Winkler, Phys. Rev. E **64**, 016408 (2001).
[38] Webpage: http://www.scipy.org (open-source software for mathematics, science, and engineering).
[39] M.-K. Chen, Phys. Rev. A **56**, 4537 (1997).
[40] Search in our group's web page http://gfam.udea.edu.co.
[41] J. W. Cooper, U. Fano, and F. Prats, Phys. Rev. Lett. **10**, 518 (1963).
[42] C. D. Lin, Phys. Rev. A **29**, 1019 (1984).
[43] S. B. Zhang, J. G. Wang, and R. K. Janev, Phys. Rev. Lett. **104**, 023203 (2010); Phys. Rev. A **81**, 032707 (2010).
[44] Y. K. Ho and S. Kar, Few-Body Syst. **53**, 445 (2012).